frontiers | Frontiers in Physics

TYPE Original Research
PUBLISHED 19 November 2024
DOI 10.3389/fphy.2024.1497267

OPEN ACCESS

EDITED BY
Marco Mandurrino,
National Institute of Nuclear Physics of Turin, Italy

REVIEWED BY
Simone Michele Mazza,
University of California, Santa Cruz, United States
Markus Kuster,
European X-Ray Free Electron Laser, Germany

*CORRESPONDENCE
A. Lampis,
andrea.lampis@ca.infn.it

RECEIVED 16 September 2024
ACCEPTED 21 October 2024
PUBLISHED 19 November 2024

CITATION
Addison M, Bellora A, Borgato F, Brundu D, Cardini A, Cossu GM, Dalla Betta GF, La Delfa L, Lai A, Lampis A, Loi A, Obertino MM, Vecchi S and Verdoglia M (2024) Characterisation of 3D trench silicon pixel sensors irradiated at $1{\cdot}10^{17}$ 1 MeV n_{eq} cm^{-2}. *Front. Phys.* 12:1497267. doi: 10.3389/fphy.2024.1497267

Characterisation of 3D trench silicon pixel sensors irradiated at $1{\cdot}10^{17}$ 1 MeV n_{eq} cm^{-2}

M. Addison[1], A. Bellora[2,3], F. Borgato[4,5], D. Brundu[6,7], A. Cardini[6], G. M. Cossu[6], G. F. Dalla Betta[8,9], L. La Delfa[6], A. Lai[6], A. Lampis[6]*, A. Loi[6], M. M. Obertino[2,3], S. Vecchi[10] and M. Verdoglia[6,5]

[1]Department of Physics and Astronomy, University of Manchester, Manchester, United Kingdom, [2]INFN, Sezione di Torino, Torino, Italy, [3]Dipartimento di Scienze Agrarie, Forestali e Alimentari, Università di Torino, Torino, Italy, [4]INFN, Sezione di Padova, Padova, Italy, [5]Dipartimento di Fisica, Università di Padova, Padova, Italy, [6]INFN, Sezione di Cagliari, Cagliari, Italy, [7]Dipartimento di Fisica, Università di Cagliari, Cagliari, Italy, [8]TIFPA INFN, Trento, Italy, [9]Dipartimento di Ingegneria Industriale, Università di Trento, Trento, Italy, [10]INFN, Sezione di Ferrara, Ferrara, Italy

The 3D trench silicon pixel sensors developed by the *TimeSPOT* collaboration have demonstrated exceptional performance, even after exposure to extreme radiation fluences up to $1 \cdot 10^{17}\,1\,\mathrm{MeV\,n_{eq}/cm^2}$. This study assesses the radiation tolerance of these sensors using minimum ionizing particles during a beam test campaign. The results indicate that while radiation damage reduces charge collection efficiency and overall detection efficiency, these losses can be mitigated to levels comparable to non-irradiated sensors by increasing the reverse bias voltage. Charge multiplication was observed and characterised for the first time in 3D trench sensors, revealing a distinct operating regime post-irradiation achievable at bias voltages close to 300 V. Additionally, the timing performance of irradiated sensors remains comparable to their non-irradiated counterparts, underscoring their resilience to radiation damage. Currently, 3D trench silicon detectors are among the fastest and most radiation-hard pixel sensors available for vertex detectors in high-energy physics colliders. These findings highlight the potential of these sensors for new 4D tracking systems of future experiments at the Future Circular Hadron Collider (FCC-hh), advancing the capabilities of radiation-hard sensor technology.

KEYWORDS

particle tracking detectors, solid-state detectors, timing detectors, 4D tracking, radiation hardness, high time resolution, high luminosity, FCC-hh

1 Introduction

Tracking particles at extremely high fluences is one of the primary challenges for future hadronic collider experiments. To cope with the $\mathcal{O}(10)$ increase in instantaneous luminosity at the High Luminosity Large Hadron Collider (HL-LHC) compared to the current LHC, several innovative detector solutions have been proposed. Among these, 3D trench silicon pixel sensors have emerged as a promising candidate due to their excellent spatial and temporal resolution, along with their radiation hardness, which was already proven up to fluences of $2.5 \cdot 10^{16}\,1\,\mathrm{MeV\,n_{eq}/cm^2}$ [1]. These sensors are particularly well-suited for high-occupancy tracking detectors operating close to

the interaction points, where traditional Low-Gain Avalanche Diode (LGAD) sensors may fail because they cannot withstand such high levels of radiation [2].

Previous studies have demonstrated that the performance of 3D trench sensors, after being subjected to irradiation fluences of up to $2.5 \cdot 10^{16}$ 1 MeV n_{eq}/cm^2, could be fully restored to pre-irradiation levels by increasing the reverse bias voltage by a few tens of volts [3]. This finding suggests that the radiation hardness of these sensors has not yet reached its upper limit. To further explore this potential, an additional irradiation campaign was conducted, extending the fluence to $1 \cdot 10^{17}$ 1 MeV n_{eq}/cm^2 to get closer to the fluences expected at the Future Circular Hadron Collider (FCC-hh) [4].

The irradiated 3D trench sensors were systematically characterised using a 180 GeV/*c* charged hadron beam from the CERN SPS/H8 beam-line. Key performance metrics including charge collection efficiency, timing performance, and detection efficiency, were evaluated and compared to those of non-irradiated sensors.

2 Materials and methods

2.1 Irradiated 3D trench sensors

3D Silicon Sensor (3DSS) technology is based on the principle that the electrodes are built within the sensor bulk in vertical structures using advanced fabrication techniques such as Deep Reactive Ion Etching (DRIE). This allows the decoupling of inter-electrode distance from wafer thickness, which consequently improves radiation hardness and time performance Parker et al. [5]. By reducing the inter-electrode distance below 30 μm, a 3D sensor is capable of collecting the same charge as a planar sensor with equivalent bulk thickness in time intervals lower by an order of magnitude. This feature gives 3D sensors enhanced timing performance compared to their planar counterparts and reduces the likelihood of charge carriers becoming trapped during the drift process, making them more radiation-hard. Within the INFN-CSN5 project *TimeSPOT* (Time and Space real-time Operating Tracker), a 3DSS has been designed with the purpose of meeting the requirements of the future vertex detectors of HL-LHC, such as the Vertex Locator of the LHCb Phase-II Upgrade [6], where a time resolution below 50 ps is required.

The sensor (Figure 1) is an *n-on-p* type with a pixel pitch of 55 μm and an active thickness of 150 μm. This geometry presents 3 wall-electrodes, two external continuous ones with a thickness of 5 μm and a depth of 150 μm which provide the bias voltage, and one centrally allocated and discontinuous readout electrode [7] inspiring the device name: 3D trench sensor. The readout electrode is designed to be smaller than the pixel pitch, with a length of 40 μm which has been considered the best compromise between maximum coverage of the electric field and minimum sensor capacitance [8]. Two sensor batches were produced by FBK in 2019 and 2021, featuring different sensor test structures and matrices, as well as an improved fabrication process for the second batch. 3D trench sensors have been fully characterised in several beam test campaigns, exhibiting a time resolution close to 10 ps and detection efficiency of 99% [9, 10, 11] while their radiation resistance was proven up to fluences of $2.5 \cdot 10^{16}$ 1 MeV n_{eq}/cm^2 [3]. A further irradiation campaign has been performed in 2023 with the aim to study the sensor behaviour and performance at even higher radiation levels. Several test structures were irradiated at the TRIGA Mark II Reactor at the Jožef Stefan Institute in Ljubljana, [12] at fluences of $5 \cdot 10^{16}$ 1 MeV n_{eq}/cm^2 and $1 \cdot 10^{17}$ 1 MeV n_{eq}/cm^2. After irradiation, the test structures were stored in a temperature-controlled box at approximately −20°C to prevent mitigation of radiation damage due to reverse annealing. Two different test structures from the second batch were wire bonded to the readout boards: the single-pixel and the triple-strip (Figure 2). In the single-pixel structure, the innermost pixel of a group of seven adjacent pixels in a row is read out, whilst the two adjacent pixels are connected to ground to ensure the proper electric field configuration. This structure is used for charge collection and timing characterisations. The triple-strip structure comprises 30 pixels arranged in three adjacent rows with their readout electrodes shorted together. Due to its larger active area, this device is used for efficiency measurements. During the beam test, the test structures were read out through the high power consumption 1 GHz bandwidth single-channel front-end electronic boards based on discrete components developed within the *TimeSPOT* project, which is described in Reference [13]. The board hosts the test structures and provides the bias voltage to the sensors by means of a conductive tape placed on the back side of the sensors.

2.2 Beam test setup

The irradiated 3D trench test structures were characterised with a 180 GeV/*c* π^+ beam during a test campaign at the SPS H8 beam-line. On average, the beam contained 10^6 particles extracted every 30 s in a 4-second-long spill and was focused into a circular spot with less than 8 mm radius at the location of the experimental setup. The setup, shown in Figure 3, allows up to three silicon detectors to be installed in three movable stations, placed inside a light-tight and electromagnetically shielded dark enclosure. Two Micro-Channel-Plate Photo-Multiplier Tubes (MCP-PMTs), aligned along the beam line, served as timing reference for the particles, providing a time of arrival with 3–4 ps accuracy when combined [14]. The station at the centre of the enclosure, Station 2, hosted the DUT and was kept at low temperature through the use of dry ice. To monitor the temperature of the DUT a PT 100 sensor was used. Few hundreds grams of dry ice, together with station insulation using a polystyrene box, allowed sensors to be tested in a temperature range [−40, −20]°C for more than 12 h without the need to refill the dry ice. The cooled station was mounted on a remotely controllable closed-loop piezoelectric rotation stage, in order to test the sensors at different tilt angles with respect to the beam direction with 35 μrad accuracy. Stations 1 and 3, placed before and after the cooled station respectively, were mounted on movable closed-loop piezoelectric linear stages that allowed transversal movements with respect to the beam line with an accuracy of 25 nm[1].

1 https://www.newport.com/p/CONEX-SAG-LS32

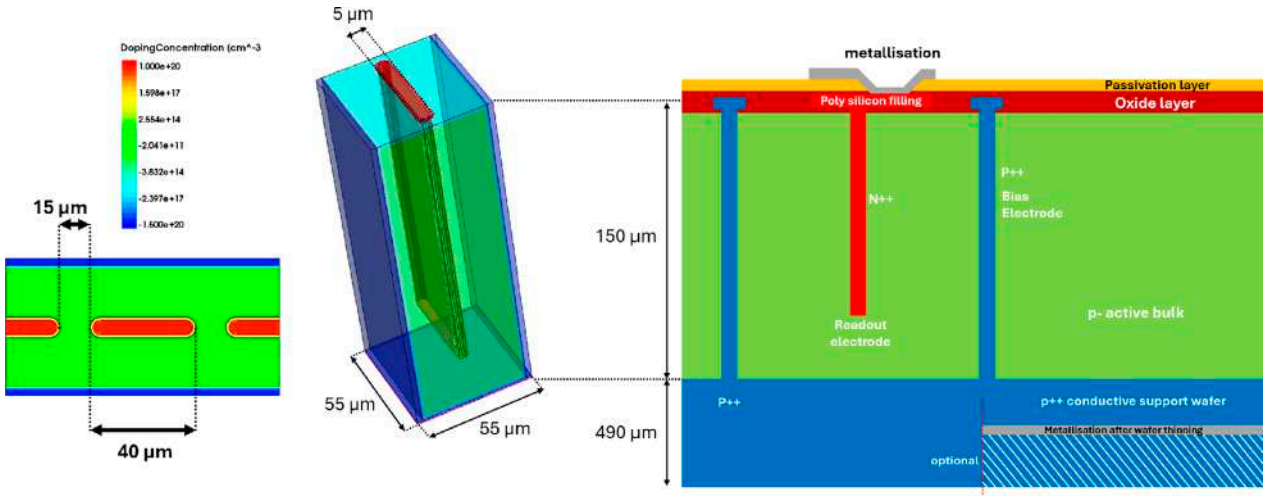

FIGURE 1
Structure and technological profile of the 3D trench sensor developed within the *TimeSPOT* project.

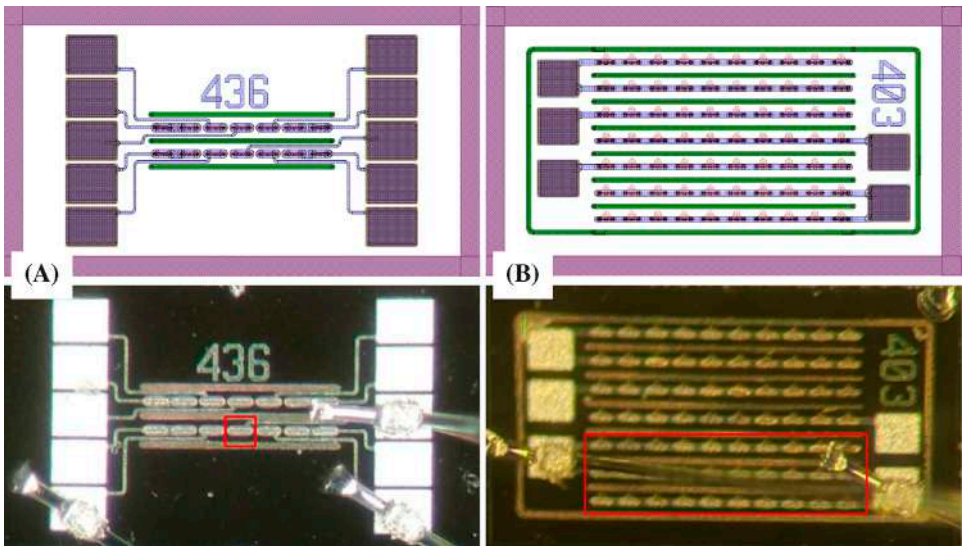

FIGURE 2
Layout and pictures of the 3D trench test structures tested at the CERN SPS: the single-pixel sensor **(A)** and the triple-strip sensor **(B)**. For each structure the active area is outlined in red and is equal to 55 µm × 55 µm for the single-pixel and 165 µm × 550 µm for the triple-strip sensor.

Two station configurations were used: one for measuring the detection efficiency and the other for the charge collection efficiency and time resolution measurements. The setup for the detection efficiency (Figure 3C) included two non-irradiated pixels positioned in Stations 1 and 3 and one of the two MCP-PMTs. In this configuration, the trigger condition required a coincidence of signals from both Stations 1 and 3, while the DUT consisted of triple-strip irradiated at a given fluence. For time resolution and charge collection efficiency measurements, the pixel at Station 3 was removed (Figure 3A), and a second MCP-PMT was included in the acquisition to provide a more accurate time reference. In this configuration, the trigger condition was the coincidence of signals from Station 1 and one of the two MCP-PMTs, and the DUTs were single-pixel irradiated structures.

The signals from the silicon sensors and the MCP-PMTs were recorded by an 8 GHz analog bandwidth 20 GSa/s four-channels digital oscilloscope. The connection of the detectors to the oscilloscope was made through low-loss RF coaxial cables. The coincidence for the triggers required signals with a minimum amplitude in two detectors inside a time window of 20 ns. The trigger conditions used for both setup configurations avoid biases in the DUT, which was never included in the acquisition condition. An example of signals acquired for the efficiency measurements is shown in Figure 4.

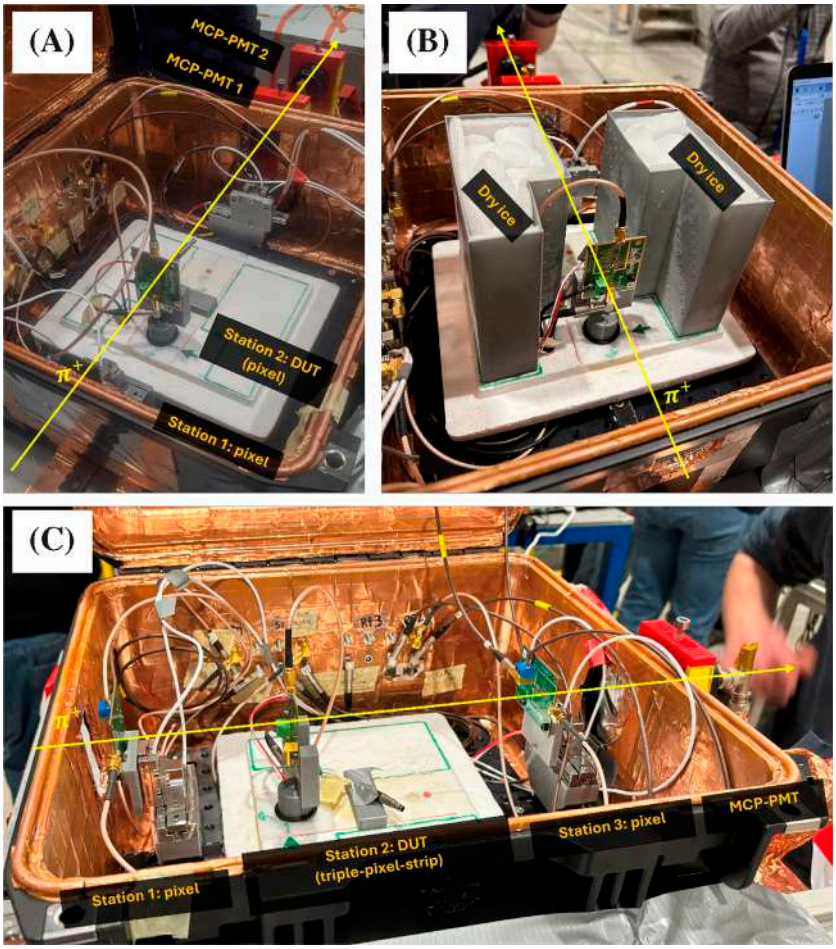

FIGURE 3
Pictures of test beam setups. **(A)** Charge collection efficiency and time resolution setup, with a single-pixel in Station 1 aligned to the DUT in Station 2; the two MCP-PMTs are also visible. **(B)** Front view of the light-tight box, where the containers fully filled with dry ice are visible. **(C)** Detection efficiency setup: the two single-pixels in Stations 1 and 3 are carefully aligned with respect to the triple-strip sensor (DUT), and the single MCP-PMT is visible outside the box. The yellow lines represent the beam direction.

2.3 Analysis method

The analysis strategy is similar to that followed in previous test beam campaigns and is discussed in References [3, 9, 10]. The waveforms acquired by the oscilloscope were automatically saved as a time series of voltage samples, which were further processed using various software algorithms. To determine the signal amplitude, the baseline value was first calculated by fitting the initial samples of the waveform on an event-by-event basis with a constant function. The final amplitude was then obtained by subtracting this baseline value from the minimum value of the waveform. Different methods have been studied in past analyses for signal time measurement. In this analysis, two methods were used: the reference method and the spline method. The reference method applies the amplitude and rise-time compensation (ARC) algorithm [15], i.e., the signal waveform is delayed by approximately half of the signal rise-time, and a subtraction between the original and delayed waveform is performed, resulting in a new waveform with reduced correlated noise. The Time of Arrival (TOA) is then determined as the point where the subtracted waveform exceeds half of its maximum amplitude. The spline method refines the constant-fraction discrimination approach. To improve accuracy and reduce sensitivity to time digitization, the samples were first interpolated with a cubic spline, and the TOA was then determined as the point of the spline function corresponding to 20% of the peak amplitude. Although the reference method provides the best time resolution performance, the spline method is applied to obtain results with an algorithm potentially similar to a constant fraction discriminator that can be implemented in front-end electronics. After this pre-processing, the resulting dataset, containing all events with their corresponding amplitude and time measurements, is further statistically analysed as explained in the following sections.

2.3.1 Charge collection efficiency

Irradiation typically leads to a reduction in the Charge Collection Efficiency (CCE) of silicon sensors. To evaluate possible changes in the 3D trench pixels response after irradiation, the CCE analysis was performed on several test structures: non-irradiated, irradiated at $5 \cdot 10^{16}\,1\,\mathrm{MeV\,n_{eq}/cm^2}$ and $1 \cdot 10^{17}\,1\,\mathrm{MeV\,n_{eq}/cm^2}$ operated at different bias voltages. The results from a previous beam

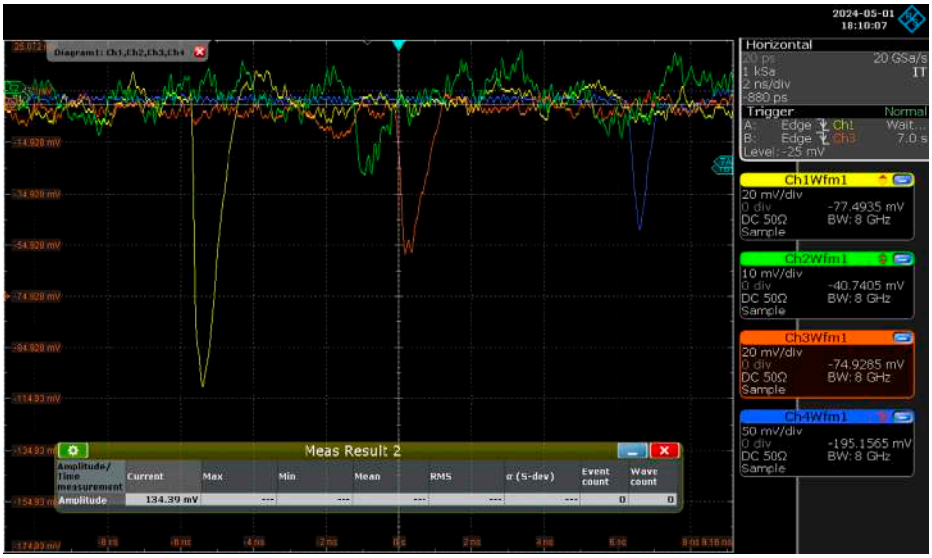

FIGURE 4
A typical event from the oscilloscope display in which a charged particle crosses the four detectors of the setup used for the efficiency measurements. The signals from the two triggering pixels are shown in yellow and orange, the signal of an irradiated triple-strip sensor is showed in green, while the signal from the MCP-PMT is reported in blue.

test characterisation on non-irradiated pixels [10] were used as a reference. Charge collection is inferred from the signal amplitudes, assuming the electronic amplifier has a linear response in charge. Due to the fast shaping-time of the amplifier, some deviation from linearity is expected for the slower signals, caused by the ballistic deficit. However, this deviation is estimated to be negligible for typical 3D trench sensor signals; moreover, any presence of ballistic deficit would only result in a decrease in the collected charge. The amplitude-to-charge calibration was performed by comparing the measured amplitude distribution of the non-irradiated sensor with the charge spectrum from simulations for different test structures and operating points. The simulations accurately model the particle beam conditions at SPS and their interaction with the 3D trench sensor using GEANT4 and TCoDe packages [11, 16].

The calibration factor is calculated as the ratio of Most Probable Value (MPV) of the distributions of the charge in simulation and of the measured amplitude in data. The MPVs are obtained by fitting the distributions with a Landau probability density function convolved with a Gaussian function that models the smearing in data due to amplifier noise. A check on the calibration factor was done using samples corresponding to different tilt angles, where different charge deposits are expected. The results agree within uncertainties, and validate the assumption of a linear behaviour of the amplifier. The charge collection distribution are then obtained for all the tested structures by multiplying the signal amplitudes for the calibration factor. To account for the fact that irradiated sensors were tested at low temperatures, while the calibration factor is determined using data taken at room temperature, the amplifier gain variation as a function of temperature was studied using a climatic chamber at the INFN Cagliari laboratories. With respect to room temperature, a 6 – 8% increase in gain was observed in the beam test temperature range $[-40, -20]$°C. As a consequence, the calibration factor of each measurement was also corrected to account for the average temperature at which the sensors were operated. To determine the MPV, the charge distribution is fitted with a Landau function convolved with a Gaussian. The obtained MPV and the Full Width at Half Maximum (FWHM), extracted from the distribution, are analysed as a function of the sensor bias voltage. The results for both parameters are discussed in Section 3.1 for the two different irradiation fluences.

2.3.2 Detection efficiency

Measurements of detector efficiency were performed using tracks hitting two 3D trench pixels along the beam line and a triple-strip as a DUT. The two single-pixels acted as the trigger whilst the time reference was provided by a single MCP-PMT. To minimise the overlap of the trench electrodes, the triple-strip was oriented such that its trenches were perpendicular to those of the trigger pixels.

The sensor efficiency ϵ is defined as the ratio of the number of tracks detected by the DUT N_{DUT} to the number of triggered tracks N_{T} (Equation 1).

$$\epsilon = \frac{N_{\mathrm{DUT}}}{N_{\mathrm{T}}}. \tag{1}$$

A track is considered detected by the DUT if its measured TOA is consistent with the expected time of flight. For this analysis the TOA of the DUT is reconstructed using the spline method. A histogram of the TOA difference between a triple-strip and the MCP-PMT for all triggered events is shown in Figure 5. The events detected by the DUT are located within the peak of the distribution, which is modeled by the sum of a Gaussian function and an exponential function convolved with a Gaussian. The non-detected tracks are reconstructed with a random TOA value, which follows a uniform distribution.

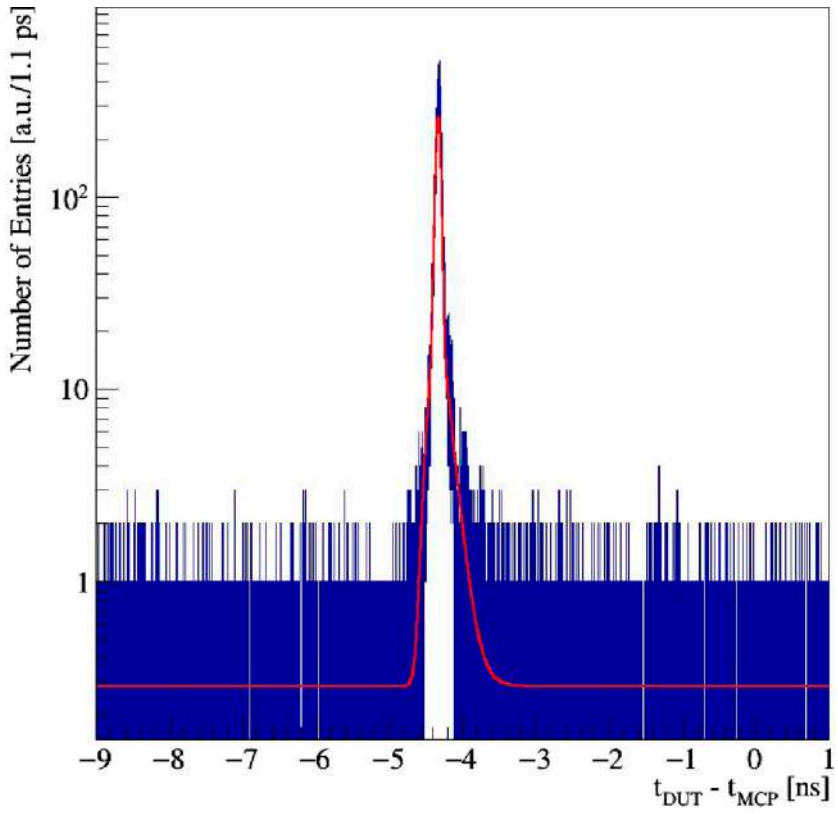

FIGURE 5
Distribution of the time difference between the triple-strip (DUT) and the MCP-PMT. The fit result is represented by the red line.

2.3.3 Time resolution

To accurately determine the DUT time resolution, the acquisition was triggered by the coincidence of signals detected in the single-pixel at Station 1 and in one of the two MCP-PMTs located downstream of the DUT. As explained in Section 2.2, the four devices were carefully aligned to maximize the rate of detected coincidences. The final measurement of time resolution is made with respect to the time reference given by the mean of the TOAs of the two MCP-PMTs ($\langle t_{\mathrm{MCP-PMTs}} \rangle$), both evaluated with the spline method, which has an accuracy of about 4 ps. The difference in TOA of the DUT (t_{Si}) and $\langle t_{\mathrm{MCP-PMTs}} \rangle$ is computed for both the reference and spline methods. From previous analyses, it was expected that the profile of the signal time distribution features a narrow peak followed by a small tail due to late signals. Similarly to what discussed in Section 2.3.2, for the efficiency measurement, noisy and non-reconstructed signals contribute to a flat background distribution which is uncorrelated in time with respect to the time reference. For this reason, the time distribution is fitted by the sum of two Gaussian functions, which describes the two components of a well-reconstructed signal, as well as a constant function for the background. This approach has been supported by first principle simulations as described in Reference [17]. Finally, the time resolution of the single-pixel σ_{Si} is obtained as the square root of the difference in quadrature between the effective variance of the signal model and the variance of the time reference distribution.

3 Results

3.1 Charge collection efficiency

To investigate the charge collection reduction and its mitigation by the increasing of the bias voltage, the charge collected by two 3D trench single-pixel structures irradiated at $5 \cdot 10^{16}$ 1 MeV n_{eq}/cm^2 and $1 \cdot 10^{17}$ 1 MeV n_{eq}/cm^2 have been studied for several bias voltages. In Figure 6, the charge collection distributions, obtained with the conversion described in Section 2.3.1 for different irradiation levels and at different bias voltages are shown and compared to those of a non-irradiated pixel from Reference [10]. The distributions of the irradiated pixels follow a Landau shape, similar to those of the non-irradiated sensor. While the non-irradiated pixel shows similar charge distributions starting from 50 V, the irradiated sensors exhibit greater discrepancies in charge collection performance, even at higher bias voltages, indicating reduced charge collection efficiency.

Both irradiated pixels show a recovery in charge collection performance as the reverse bias voltage is increased, with the $5 \cdot 10^{16}$ 1 MeV n_{eq}/cm^2 showing full recovery below 250 V and the $1 \cdot 10^{17}$ 1 MeV n_{eq}/cm^2 at about 275 V, as visible from the charge distributions in Figure 7. The small discrepancy observed at low ke it can be attribute to the higher noise of the front-end amplifier electronics due to the increased leakage current of irradiated pixels. Furthermore, when operated at a reverse bias voltage close to 300 V

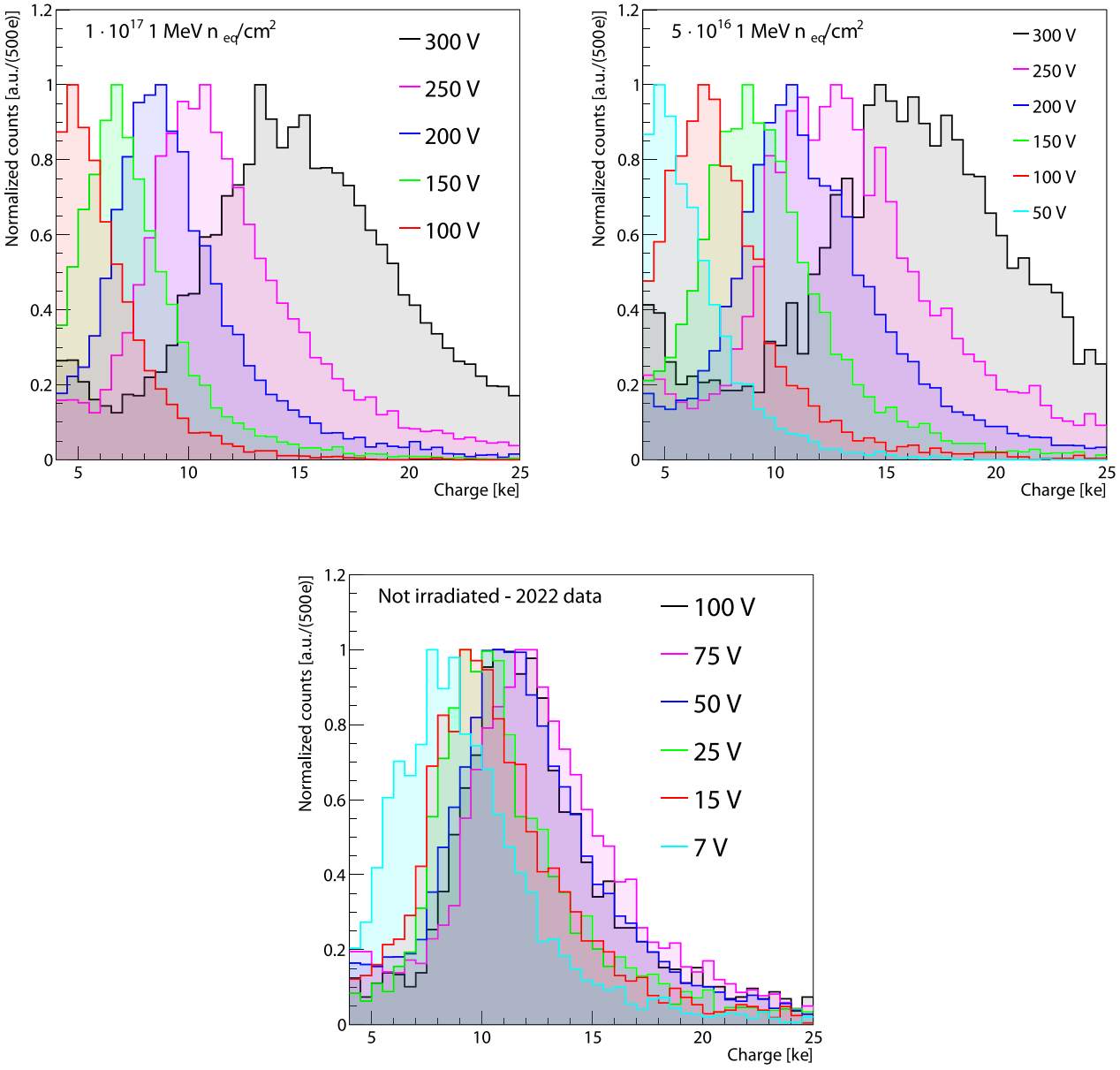

FIGURE 6
Normalized charge distributions, in electrons unit, as a function of bias voltage. (Top left) irradiated sensor at $1 \cdot 10^{17}$ 1 MeV n_{eq}/cm^2 and (Top right) $5 \cdot 10^{16}$ 1 MeV n_{eq}/cm^2, (bottom) non-irradiated sensor (from Reference Borgato et al. [10]). The distributions correspond to the detection of positive hadrons with a momentum of 180 GeV/*c*.

the charge distributions for both pixels peak to higher values than the one of the non-irradiated and a broadening of the distributions is also observed, providing evidence of charge multiplication. This is the first time this effect has been observed in 3D trench sensors. Charge multiplication effects were in fact observed in double-sided columnar 3D sensors irradiated to fluences of the order of 10^{15} 1 MeV n_{eq}/cm^2 and operated at high voltage [18]. In these devices, the inter-electrode distance was $L \simeq 56$ μm and charge multiplication took place at a voltage of the order of 250 V. More recently, charge multiplication was observed in single-sided columnar 3D sensors irradiated to fluences of the order of 10^{16} 1 MeV n_{eq}/cm^2 [19]. Due to the smaller value of $L \simeq 35$ μm, this effect was anticipated at a reverse voltage of about 125 V. In all these devices, the onset of charge multiplication has been mainly attributed to the high electric field peaks developing at the read-out junction electrode tips, as confirmed by TCAD simulations [20]. In spite of the very small inter-electrode distance ($L = 27.5$ μm), charge multiplication had not been observed in 3D trench sensors irradiated at lower fluences. The reason for this difference is mainly attributed to the larger maximum reverse voltages applied in the present study in order to boost the sensor performance. Such bias voltages were not used in previous tests because the efficiency and timing resolution of samples irradiated up to $2.5 \cdot 10^{16}$ 1 MeV n_{eq}/cm^2 could be fully recovered at 150 V [3].

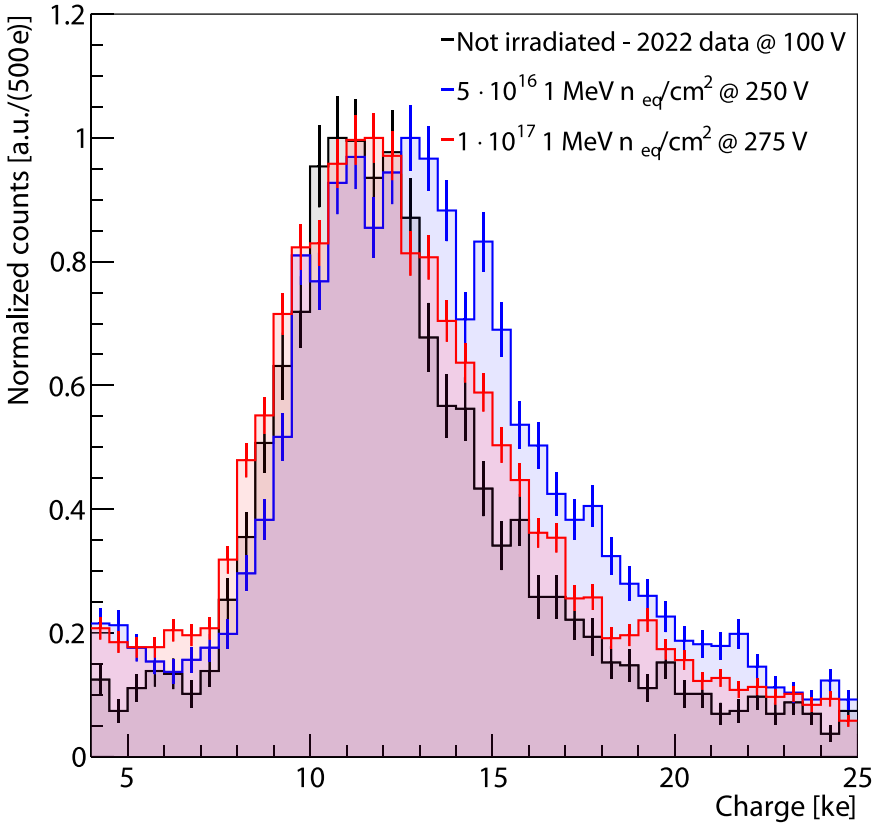

FIGURE 7
Normalized charge distributions, in electrons unit, of the $1 \cdot 10^{17}$ 1 MeV n_{eq}/cm^2 pixel operated at a reverse bias of 275 V and the $5 \cdot 10^{16}$ 1 MeV n_{eq}/cm^2 at 250 V, compared to the one of a non-irradiated pixel operated at 100 V.

To make quantitative comparisons of charge collection efficiencies for the tested sensors, the MPVs of the charge distributions were plotted as a function of reverse bias voltage, as shown in Figure 8. Both irradiated sensors exhibit a similar trend, with the most irradiated one showing lower charge collection efficiency. In contrast, the non-irradiated sensor shows no significant dependence on reverse bias voltage beyond 50 V. The comparison of the MPVs indicates a full recovery of charge collection efficiency for both irradiated sensors, as qualitatively inferred from the distributions. Additionally, it reveals that sensors with higher irradiation levels require a greater reverse bias voltage to achieve this recovery.

When operating the sensors at higher bias voltages, close to 300 V, multiplication factors of approximately 1.4 for the $5 \cdot 10^{16}$ 1 MeV n_{eq}/cm^2 and 1.2 for the $1 \cdot 10^{17}$ 1 MeV n_{eq}/cm^2 sensor were observed, along with a significant increase in the FWHM of the charge distributions.

3.2 Detection efficiency

Detection efficiency was evaluated using the method detailed in Section 2.3.2. Since the trigger setup differed from that used in previous measurements [3, 10], the results with the new layout were first validated by measuring the efficiency of a non-irradiated sensor as a function of the incident beam angle. These results were found to be consistent with those reported in Reference [3], which are more comprehensive and will therefore be used for comparison with the new measurements in this article. The dependence of 3D trench detection efficiency on the tilt angle relative to normal incidence has been previously demonstrated [3, 10]. Since the trench electrodes are non-sensitive volumes, a recovery of detector efficiency is expected when tilting a 3D trench sensor with respect to the beam path. This effect has also been studied for the $1 \cdot 10^{17}$ 1 MeV n_{eq}/cm^2 triple-strip sensor, and Figure 9 (left) shows the results obtained for that structure operated at a reverse bias voltage of 250 V, as well as those reported in Reference [10] for a non-irradiated device. Both sets of measurements exhibit a similar trend, characterised by an initial sharp increase up to 10°, followed by a more gradual rise. Specifically, for the sensor irradiated at $1 \cdot 10^{17}$ 1 MeV n_{eq}/cm^2, the efficiency increases from (77.4 ± 0.5)% at 0° to (90.8 ± 0.6)% at 10°and reaches (94.6 ± 0.6)% at 20°.

The impact of bias voltage on detection efficiency for the triple-strip irradiated at $1 \cdot 10^{17}$ 1 MeV $n_{eq}/cm^2$was investigated by varying the reverse bias from 100 V to 270 V. The results of two voltage scans for two incident beam angles 0° and 20° for the $1 \cdot 10^{17}$ 1 MeV n_{eq}/cm^2 triple-strip, as well as a single measurement for the $5 \cdot 10^{16}$ 1 MeV n_{eq}/cm^2 at 200 V and normal beam incidence are shown in Figure 9 (right). As expected, detection efficiency increases with reverse bias voltage. At a tilt angle of 0°, the sensor irradiated at $1 \cdot 10^{17}$ 1 MeV n_{eq}/cm^2 achieves a detection efficiency

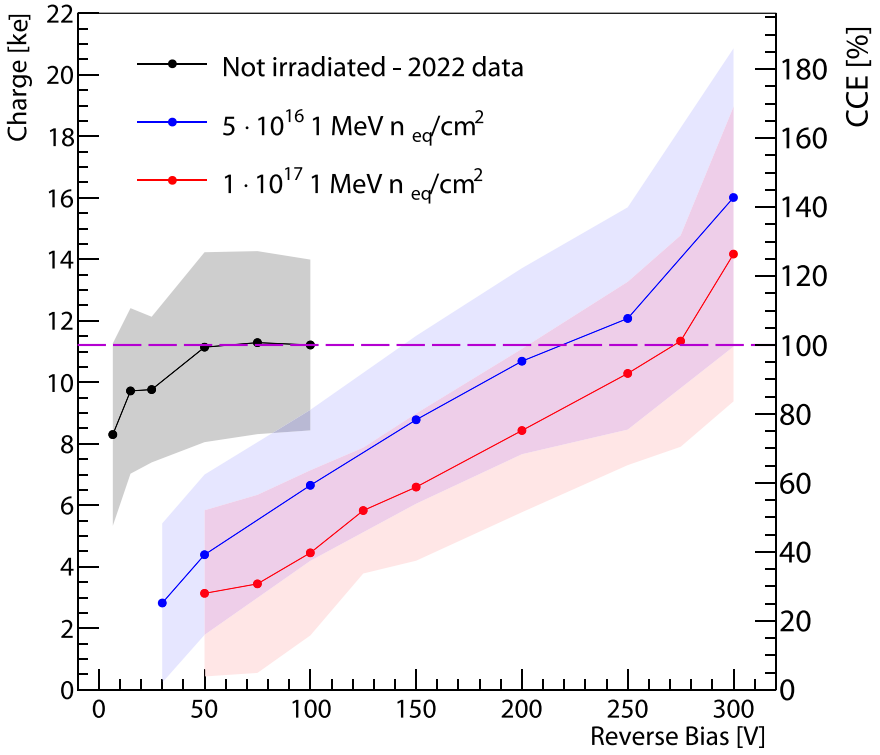

FIGURE 8
MPV of the charge distributions and Charge Collection Efficiency for the two irradiated and for the non-irradiated pixels as a function of the reverse bias voltage. The 100 V MPV data of the non-irradiated pixel have been used as a reference for the CCE evaluation. The colored areas represent the FWHM of the distributions.

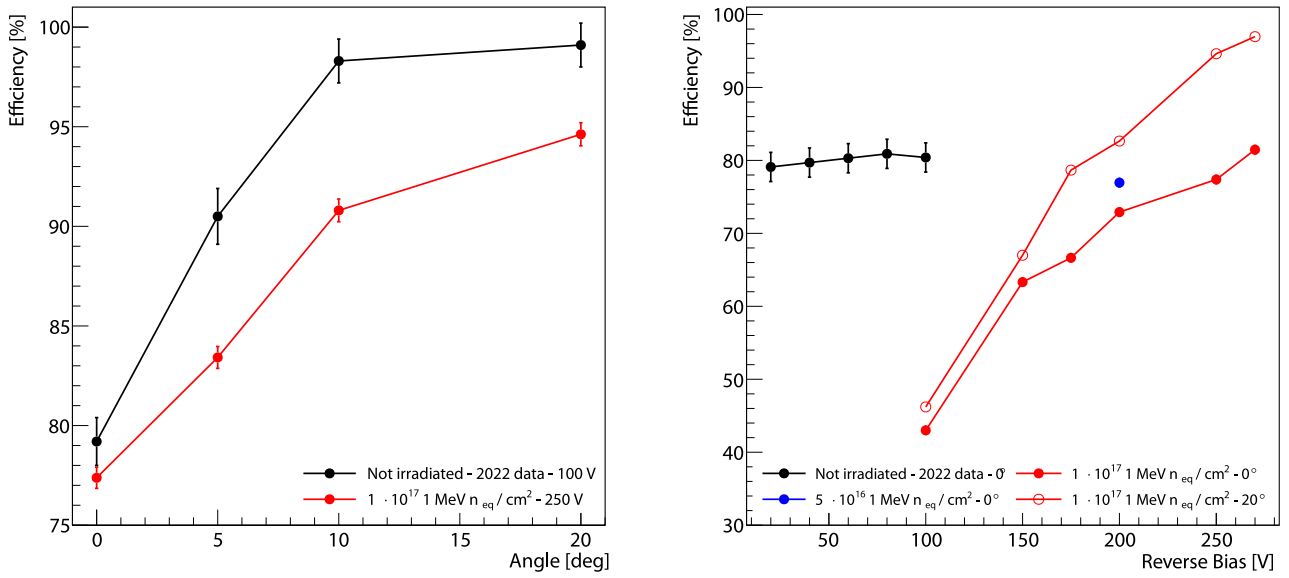

FIGURE 9
(Left) Detection efficiency as a function of tilt angle for a triple-strip sensor irradiated at $1 \cdot 10^{17}$ 1 MeV n_{eq}/cm^2 at a reverse bias voltage of 250 V.(Right) Detection efficiency versus reverse bias voltage for triple-strip sensors irradiated to $5 \cdot 10^{16}$ 1 MeV n_{eq}/cm^2 and $1 \cdot 10^{17}$ 1 MeV n_{eq}/cm^2. In both plots, results for a non-irradiated sensor obtained in a previous test beam campaign, as described in Reference Borgato et al. [3], are also included.

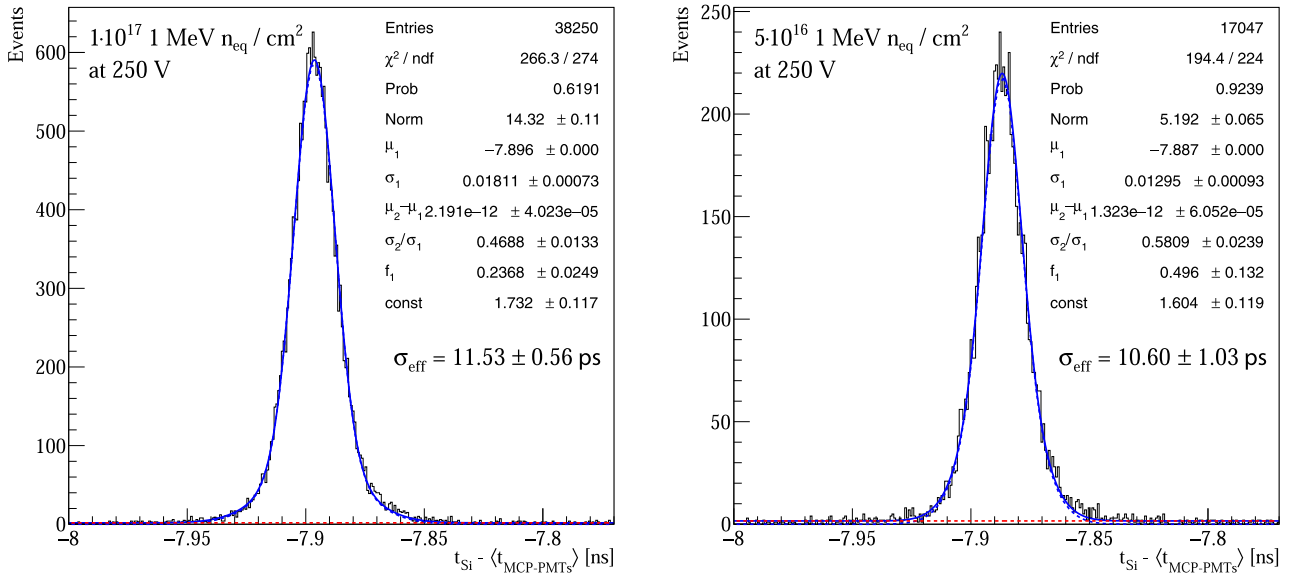

FIGURE 10
Distributions of the difference between the time of arrival of the 3D trench single-pixel (reference method) and the time reference, $t_{Si} - \langle t_{\text{MCP-PMTs}} \rangle$, for the pixel irradiated at (left) $1 \cdot 10^{17}$ 1 MeV n_{eq}/cm^2 and (right) $5 \cdot 10^{16}$ 1 MeV n_{eq}/cm^2, both operated at reverse bias of 250 V.

comparable to that of the non-irradiated sensor once the reverse bias voltage exceeds 250 V. In the bias voltage scan at 20° the $1 \cdot 10^{17}$ 1 MeV n_{eq}/cm^2 sensor exhibits higher detection efficiencies, reaching a maximum of (96.8 ± 0.6)% at 270 V, which is about 2% lower than the 99% reached by the non-irradiated one for the same tilt angle. Furthermore, the detection efficiency of the triple-strip irradiated at $5 \cdot 10^{16}$ 1 MeV n_{eq}/cm^2 at a reverse bias voltage of 200 V is found to be between the measurements of the non-irradiated sensor and the $1 \cdot 10^{17}$ 1 MeV n_{eq}/cm^2 triple-strip operated at the same bias voltage, in agreement with the charge collection efficiency results.

Consistently, these measurements, along with those shown in the charge collection efficiency study, demonstrate that 3D trench sensors irradiated at very high fluences achieve similar detection performance to that of a non-irradiated sensor if operated at a sufficiently high reverse bias voltage.

3.3 Time resolution

This section reports the results of the time resolution studies on two 3D trench single-pixels irradiated at $5 \cdot 10^{16}$ 1 MeV n_{eq}/cm^2 and $1 \cdot 10^{17}$ 1 MeV n_{eq}/cm^2, at different bias voltages. The analysis method is detailed in Section 2.3.3. In Figure 10, the distributions of the difference in the TOA for the two single-pixels, both operated at a reverse bias of 250 V, are shown. As expected, the distributions are similar to one another and to the distribution of non-irradiated pixels studied in previous analyses [3, 10]. The variance of the distribution is obtained as the effective standard deviation of the Gaussian mixture as $(\sigma_t^{\text{eff}})^2 = f_1(\sigma_1^2 + \mu_1^2) + (1 - f_1) \cdot (\sigma_2^2 + \mu_2^2) - \mu^2$, where f_1 is the fraction of the first Gaussian and μ is defined as $\mu = f_1\mu_1 + (1 - f_1) \cdot \mu_2$ [10]. After subtracting the time reference contribution of the MCP-PMTs, the time resolution of the 3D trench sensors for both irradiation conditions and as a function of the reverse bias voltage is obtained. The results are shown in Figure 11 for both discrimination methods, where the results from the 2022 beam test of non-irradiated pixels are also reported for comparison. Whilst the irradiated sensors were operated in a temperature range of [−40, −20]°C, the non-irradiated sensors were operated at room temperature.

The sensors irradiated up to $1 \cdot 10^{17}$ 1 MeV n_{eq}/cm^2 have comparable time resolution to the non-irradiated ones for both discrimination methods, showing clearly that the time performance of 3D trench sensors is not significantly affected by radiation damage up to extreme fluences. As discussed in previous sections, it is necessary to increase the reverse bias for irradiated sensors to achieve the same performance in terms of efficiency and charge collection as non-irradiated sensors. Specifically, at 250 V bias, the time resolutions are (10.1 ± 1.0) ps and (10.7 ± 0.6) ps for the $5 \cdot 10^{16}$ 1 MeV n_{eq}/cm^2 and $1 \cdot 10^{17}$ 1 MeV n_{eq}/cm^2 respectively, using the reference method. These can be compared with (12.0 ± 0.7) ps for the non-irradiated pixel at 100 V.

The trend in Figure 11 shows that the time resolution does not improve significantly once the reverse bias voltage has surpassed 200 V. By further increasing the voltage to 300 V, a degradation in time resolution is observed, most likely due to impact ionization within the sensor, as previously discussed in Section 3.1. Moreover, by using the spline method, a slightly better timing performance it is observed for the sensors irradiated at $5 \cdot 10^{16}$ 1 MeV n_{eq}/cm^2 compared to the non-irradiated ones, although the results are compatible within the uncertainty. These fluctuations could be related to the different performance of the front-end electronics boards used for the different sensors, particularly due to the different temperature conditions which, as stated in Section 2.3.1, could affect the gain of the amplifier electronic up to 8%.

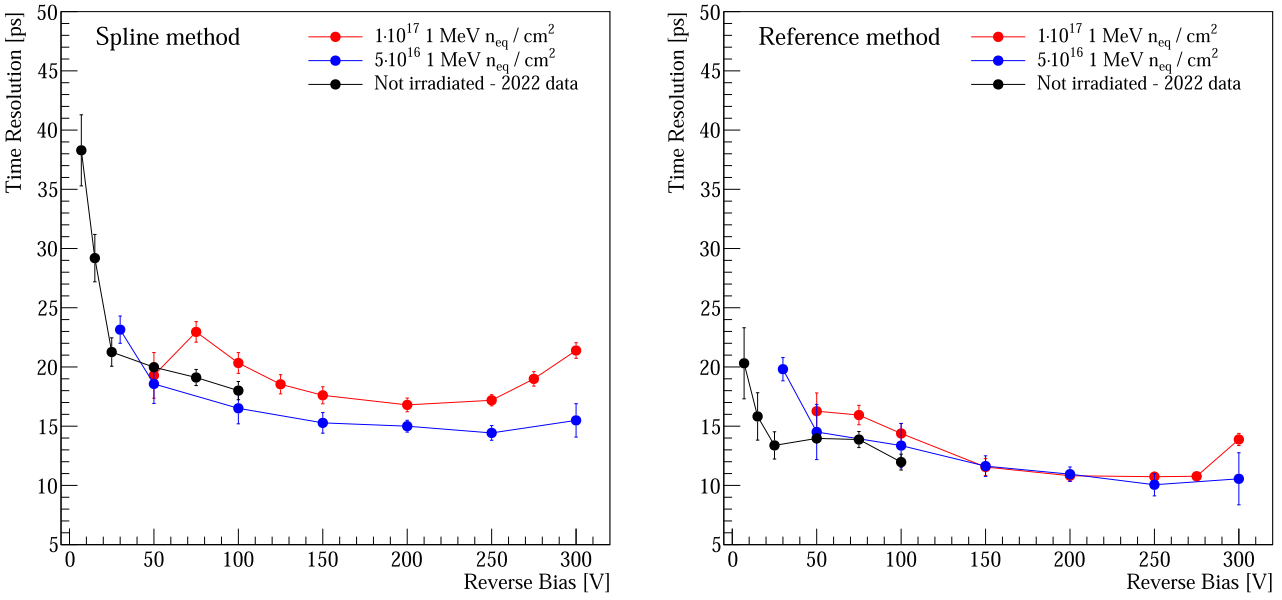

FIGURE 11
Time resolution of the single-pixels as a function of the reverse bias voltage for the different irradiation fluences obtained with the (right) reference method and (left) spline method. The contribution due to the resolution of the time reference is subtracted.

4 Discussion

The 3D trench silicon pixel sensors developed by the *TimeSPOT* collaboration have demonstrated remarkable performance in detecting high-energy charged particles, even after exposure to extreme radiation fluences. This study assessed the radiation tolerance of these sensors up to fluences of $1 \cdot 10^{17}\,1\,\mathrm{MeV\,n}_{eq}/\mathrm{cm}^2$, using minimum ionizing particles during a beam test campaign. Although radiation damage leads to a reduction in charge collection efficiency and overall detection efficiency at reverse bias voltages below 250 V, this loss is compensated by restoring charge collection and detection efficiency with higher reverse bias voltages. This finding is supported by the charge collection distribution of single-pixel sensors, where a reverse bias voltage of 275 V yields results indistinguishable from those of non-irradiated pixels. Similarly the detection efficiency of the $1 \cdot 10^{17}\,1\,\mathrm{MeV\,n}_{eq}/\mathrm{cm}^2$ triple-strip is very close to that of the non-irradiated sensor with a small degradation of about 2% when operated at 20° with respect to the beam direction. Additionally, charge multiplication was observed and studied for the first time in 3D trench sensors, revealing a new working regime achievable with this sensor technology after irradiation. Crucially, the time resolution of the irradiated sensors, measured at about 10 ps, is comparable to that of their non-irradiated counterparts, highlighting the minimal impact of radiation damage on timing accuracy, even at these unprecedented fluences.

Currently, 3D trench silicon detectors are among the fastest and most radiation-hard pixel sensors available for use in vertex detectors at high-energy physics colliders. The findings of this study further enhance the potential of these sensors for integration into the tracking systems of experiments at the Future Circular Hadron Collider (FCC-hh). This shifts the focus towards the development of low-power consumption readout ASICs for new vertex detectors, capable of meeting the enhanced radiation hardness standards set by 3D trench sensors.

Data availability statement

The raw data supporting the conclusions of this article will be made available by the authors, without undue reservation.

Author contributions

MA: Formal Analysis, Investigation, Methodology, Writing–original draft, Writing–review and editing. AB: Formal Analysis, Investigation, Methodology, Writing–original draft, Writing–review and editing. FB: Formal Analysis, Writing–review and editing. DB: Formal Analysis, Investigation, Methodology, Writing–original draft, Writing–review and editing. AC: Conceptualization, Investigation, Methodology, Writing–review and editing. GC: Conceptualization, Writing–review and editing. GD: Conceptualization, Writing–original draft, Writing–review and editing. LL: Investigation, Methodology, Writing–review and editing. ALi: Conceptualization, Investigation, Writing–review and editing. ALm: Conceptualization, Formal Analysis, Investigation, Methodology, Writing–original draft, Writing–review and editing. ALo: Conceptualization, Formal Analysis, Investigation, Writing–original draft, Writing–review and editing. MO: Formal Analysis, Investigation, Methodology, Writing–original draft, Writing–review and editing. SV: Formal Analysis, Investigation, Methodology, Writing–original draft, Writing–review and editing. MV: Conceptualization, Formal Analysis, Investigation, Methodology, Writing–original draft, Writing–review and editing.

Funding

The author(s) declare that financial support was received for the research, authorship, and/or publication of this article. This work was supported by the Fifth Scientific Commission (CSN5) of the Italian National Institute for Nuclear Physics (INFN), within the Project *TimeSPOT* and by the ATTRACT-EU initiative, INSTANT project. This project has received funding from the European Union's Horizon 2020 Research and Innovation programme under GA no. 101004761. This project has received funding from the European Union's Horizon Europe Research and Innovation program under Grant Agreement No 101057511 (EURO-LABS).

Acknowledgments

The authors wish to thank the staff of North Hall Area at CERN for their help in the beam-line setup and operations.

Conflict of interest

The authors declare that the research was conducted in the absence of any commercial or financial relationships that could be construed as a potential conflict of interest.

The author(s) declared that they were an editorial board member of Frontiers, at the time of submission. This had no impact on the peer review process and the final decision

Publisher's note

References

1. Lampis A. *Innovative silicon pixel sensors for a 4D VErtex LOcator detector for the LHCb high luminosity upgrade*. Cagliari U: Ph.d. thesis (2023).

2. Kramberger G, Carulla M, Cavallaro E, Cindro V, Flores D, Galloway Z, et al. Radiation hardness of thin low gain avalanche detectors. *Nucl Instr Methods Phys Res Section A: Acc Spectrometers, Detectors Associated Equipment* (2018) 891:68–77. doi:10.1016/j.nima.2018.02.018

3. Borgato F, Cardini A, Cossu GM, Dalla Betta GF, Garau M, La Delfa L, et al. Characterisation of highly irradiated 3D trench silicon pixel sensors for 4d tracking with 10 ps timing accuracy. *Front Phys* (2024) 12. doi:10.3389/fphy.2024.1393019

4. Abada A, Abbrescia M, AbdusSalam SS, Abdyukhanov I, Abelleira Fernandez J, Abramov A, et al. Fcc-hh: the hadron collider: future circular collider conceptual design report volume 3. *Eur Phys J Spec Top* (2019) 228:755–1107. doi:10.1140/epjst/e2019-900087-0

5. Parker S, Kenney C, Segal J. 3D — a proposed new architecture for solid-state radiation detectors. *Nucl Instr Methods Phys Res Section A: Acc Spectrometers, Detectors Associated Equipment* (1997) 395:328–43. doi:10.1016/S0168-9002(97)00694-3

6. The LHCb Collaboration. Framework TDR for the LHCb upgrade II: opportunities in flavour physics, and beyond. In: *Scientific committee paper* (2021).

7. Forcolin G, Boscardin M, Ficorella F, Lai A, Loi A, Mendicino R, et al. 3D trenched-electrode pixel sensors: design, technology and initial results. *Nucl Instr Methods Phys Res Section A: Acc Spectrometers, Detectors Associated Equipment* (2020) 981:164437. doi:10.1016/j.nima.2020.164437

8. Loi A. Design and test of a timing optimized 3D silicon sensor for HL-LHC experiments (2020). Available from: https://hdl.handle.net/11584/284136 (Accessed 2020).

9. Anderlini L, Aresti M, Bizzeti A, Boscardin M, Cardini A, Dalla Betta GF, et al. Intrinsic time resolution of 3D-trench silicon pixels for charged particle detection. *J Instrumentation* (2020) 15:P09029. doi:10.1088/1748-0221/15/09/P09029

10. Borgato F, Brundu D, Cardini A, Cossu GM, Dalla Betta GF, Garau M, et al. Charged-particle timing with 10 ps accuracy using TimeSPOT 3D trench-type silicon pixels. *Front Phys* (2023) 11:1117575. doi:10.3389/fphy.2023.1117575

11. Brundu D, Cardini A, Contu A, Cossu GM, Dalla Betta GF, Garau M, et al. Accurate modelling of 3D-trench silicon sensor with enhanced timing performance and comparison with test beam measurements. *J Instrumentation* (2021) 16:P09028. doi:10.1088/1748-0221/16/09/p09028

12. Lea S, Žerovnik G, Trkov A. Computational analysis of irradiation facilities at the JSI TRIGA reactor. *Appl Radiat Isot* (2012) 70:483–8. doi:10.1016/j.apradiso.2011.11.042

13. Cossu GM, Lai A. Front-end electronics for timing with pico-second precision using 3D trench silicon sensors. *J Instrumentation* (2023) 18:P01039. doi:10.1088/1748-0221/18/01/P01039

14. Lampis A. *Innovative silicon pixel sensors for a 4D VErtex LOcator detector for the LHCb high luminosity upgrade*. Cagliari, Italy: University of Cagliari (2023). PhD Thesis.

15. Cho Z, Chase R. Comparative study of the timing techniques currently employed with Ge detectors. *Nucl Instr Methods* (1972) 98:335–47. doi:10.1016/0029-554X(72)90115-2

16. Loi A, Contu A, Lai A. Timing optimisation and analysis in the design of 3d silicon sensors: the tcode simulator. *J Instrumentation* (2021) 16:P02011. doi:10.1088/1748-0221/16/02/P02011

17. Cossu GM, Brundu D, Lai A. Intrinsic timing properties of ideal 3D-trench silicon sensor with fast front-end electronics. *J Instrumentation* (2023) 18:P07014. doi:10.1088/1748-0221/18/07/P07014

18. Koehler M, Bates R, Fleta C, Jakobs K, Lozano M, Parkes C, et al. Comparative measurements of highly irradiated n-in-p and p-in-n 3D silicon strip detectors. *Nucl Instr Methods Phys Res Section A: Acc Spectrometers, Detectors Associated Equipment* (2011) 659:272–81. doi:10.1016/j.nima.2011.08.041

19. Mendicino R, Boscardin M, Dalla Betta GF. Characterization of FBK small-pitch 3D diodes after neutron irradiation up to 3.5×10^{16} n_{eq} cm^{-2}. *J Instrumentation* (2019) 14:C01005. doi:10.1088/1748-0221/14/01/C01005

20. Giacomini G, Piemonte C, Dalla Betta GF, Povoli M. Simulations of 3D detectors. In: *Proceedings of the 20th international Workshop on vertex detectors (SISSA)*. (Trieste, Italy: SISSA) (2012). p. 025.